Understanding the Unique Optical and Vibrational Signatures of Sequential Infiltration Synthesis Derived Indium Oxyhydroxide Clusters for CO_2 Absorption

Thabiso Kunene, Alex B. F. Martinson*

Materials Science Division, Argonne National Laboratory, Lemont, Illinois 60439, United States

*Email: martinson@anl.gov

1. ABSTRACT

Sequential infiltration synthesis (SIS) is a vapor phase synthesis technique with potential to exert precise control over metal oxyhydroxide incorporation into polymer scaffolds. We observe strong size-dependent properties of $InO_x(OH)_y$ few-atom clusters deposited with variable SIS cycle numbers within a polymethylmethacrylate (PMMA) matrix. Infrared and ultraviolet absorption spectroscopy reveal that the metal atom coordination and optical properties of the clusters depend on the number of SIS cycles performed as well as the choice of processing parameters. The incorporation of indium oxyhydroxide in PMMA via SIS improves the gravimetric CO_2 absorption capacity, demonstrating a novel platform with potential for CO_2 activation.

2. INTRODUCTION

Sequential infiltration synthesis (SIS) is a versatile route to hybrid organic-inorganic materials that have been transformed to purely inorganic materials templated by polymeric structures.[1–3] While SIS is inspired by atomic layer deposition (ALD) and often utilizes the same precursors and tools, SIS requires infiltration of these vapor phase precursors into a polymer film or bulk that includes reversible or irreversible interactions with polymer functional groups. In a second step, the infiltration of an oxygen source (e.g. H_2O) affords reaction to form an inorganic oxyhydroxide that may be chemisorbed at a polymer functional site or physically trapped within the polymer matrix.[4] Due to the presence of the polymer matrix, the resulting inorganic material phase is less than fully dense both before and after burnout of the polymer phase. Careful tuning of SIS conditions including temperature, precursor exposure, and the number of SIS cycles may enable a range of inorganic species ranging from single metal atom sites, to few atom clusters, to a contiguous inorganic network.[5]

A plethora of technologies ranging from catalysts to displays depend on metal oxides and hydroxides. Such crucial materials include the oxides, hydroxides and oxyhydroxides of indium that are important for optoelectronic and catalytic applications including transparent conductors, gas sensors, and electrocatalysts for CO_2 conversion.[6,7] The unique nanoscale properties of indium oxyhydroxide, including size and morphology, may provide a distinctive density of electronic states that offers novel or improved functionality in these applications.[6,8] Indium-based nanomaterials have been synthesized via a range of techniques including solvothermal synthesis and precipitation/calcination methods.[9] The SIS of $InO_x(OH)_y$ in polymethylmethacrylate (PMMA) presents a new opportunity to investigate the properties of isolated few atom $InO_x(OH)_y$ clusters at the smallest-scale. Few-atom clusters may present molecular sites that are distinct from bulk metal oxide and hydroxides due to unsaturated coordination, changes in molecular symmetry and distinct hydroxylation levels.[10–14] The unique hydroxyl groups on each SIS-grown cluster provide a model system to study indium (oxy)hydroxide surface reactivity. Better understanding of the nature of the hydroxyl groups present on indium (oxy)hydroxide clusters in the PMMA matrix may provide new catalytic pathways for and insights into transformations such as CO_2 adsorption and conversion.

We recently investigated the atomic structure and evolution of coordination environments for $InO_x(OH)_y$ nuclei formed during the earliest stages of SIS growth inside a PMMA host matrix.[15] The In K-edge EXAFS and atomic pair distribution function (PDF) analysis of high energy X-ray scattering suggest that amorphous InO_xH_y clusters possess only a few metal-atoms after 1 to 3 SIS cycles. Little is known about SIS-derived cluster diffusion, however these clusters might grow via coordinative addition and hydrolysis to form clusters with a high aspect ratio. Multinuclear clusters that result from additional SIS cycles were shown to be related to the bonding patterns found in cubic In_2O_3 and $In(OH)_3$ crystal structures. However, the use of SIS for synthesis of few-atom cluster synthesis remains in its infancy, posing several more questions raised by preliminary studies. (i) Under what conditions are undercoordinated indium-oxo clusters hydroxyl/aqua terminated? (ii) Under what conditions might

the PMMA stabilize “naked” oxo clusters through weak coordination to the carbonyl or ester functional groups in PMMA? (iii) What unique properties do few-atom indium oxyhydroxides with unique distinct cluster structure exhibit?

We further refine the synthesis of $InO_x(OH)_y$ clusters by adopting SIS process conditions in which nucleation is only feasible in the first SIS cycle, in order to favor only cluster growth (without re-nucleation) in subsequent SIS cycles. We further characterize the nature of SIS-derived $InO_x(OH)_y$ clusters as a function of size (i.e., SIS cycle number) by monitoring the vibration signatures and UV-visible absorption of clusters in PMMA. We observe striking size-dependence for hydration and hydroxylation that suggest the presence of unique surface sites that may further impact reactivity, for example with CO_2, as well as the stabilization of adsorbed species including carbonates, bicarbonates, and carbonic acid.

3. EXPERIMENTAL SECTION

Sequential Infiltration Synthesis. Silicon wafers with 300 nm thermal oxide (University Wafer) and fused quartz substrates (Technical Glass Products) were diced and subsequently cleaned by sequential sonication in acetone and isopropanol for 15 minutes followed by a 5-minute UV-ozone treatment (Jelight Company Inc., Model 18). For FT-IR experiment in reflectivity mode, a 3 nm layer of germanium followed by 100 nm layer of gold were deposited onto clean silicon substrates via thermal evaporation. PMMA thin films were prepared via spin coating at 1000 rpm for 30 seconds from 10 wt % poly(methymethacrylate) (PMMA) (Sigma-Aldrich, 99.8%) in toluene. Sequential infiltration synthesis experiments were performed in a commercial ALD reactor (Savannah 200, Veeco) equipped with a stop valve to enable extended precursor exposures. Unless otherwise mentioned, the growth chamber and precursor delivery manifold were held at 80 °C. Trimethylindium (TMIn, Strem, 98+%) was heated to 50 °C and H_2O was unheated. Safety note: trimethylindium is a pyrophoric liquid that should not be excessively heated or exposed to air. All processes were performed with a constant stream of N_2 at 5 sccm. Before beginning the SIS process, PMMA coated substrates were heated to 150 °C and outgassed in the chamber for 30 minutes under N_2 flow and rough vacuum to remove H_2O and any residual solvent as well as remove any ordered structure of PMMA. The first SIS cycle was performed with a (5-300-5-2-120-240) cycle sequence that refers to a 5 s TMIn dose that is retained in the growth chamber for an additional 300 s static exposure, a short 5 s pump and purge, followed by a 2 s H_2O dose that is retained in the growth chamber for an additional 120 s static exposure before a long 240 s pump and purge. All subsequent SIS steps were performed with a modified (5-300-120-2-120-240) cycle. The significantly longer pump/purge after TMIn dosing in all cycles after the first allow for complete dissociation of any TMIn reversibly adducted to the PMMA backbone. This approach strongly favors cluster growth in subsequent steps without addition of new nuclei on the polymer backbone. The chemistry, physics and nomenclature of SIS has been discussed elsewhere.[1,16]

Spectroscopic Ellipsometry. Variable angle ellipsometry spectra (J. A. Woollam α-SE) were acquired in the range 380-900 nm at angles 65°, 70° and 75° and analyzed using CompleteEase software. Pure PMMA films were fit to a Cauchy model using fixed optical constants (A=1.49, B=0.00125, C=0) previously deduced for PMMA. After SIS, the hybrid PMMA-indium oxyhydroxide films were fit to an effective medium approximation (EMA) layer using a Bruggeman model. This model fits the overall thickness and fraction of two Cauchy parametrized components each with fixed refraction index corresponding to PMMA and In_2O_3 (A=1.9503, B=0.036512, C=0). Good fits were obtained when refractive index parameters were held constant across all samples and the total thickness and volume fraction of indium oxyhydroxide were fit.

In-situ FTIR, DRIFTS and Gas Adsorption-Desorption Isotherms. Infrared spectra were obtained using a Bruker Vertex 70 FTIR spectrophotometer with external beam path that enters and exits the ALD tool through a modified lid fitted with an IR-transparent undoped silicon window. The reflection geometry for in situ infrared spectroscopy has been described elsewhere.[16] An external LN_2-cooled MCT-A detector and a DLaTGS detector were used to collect spectra over the 4000-400 cm^{-1} range by averaging 64 scans with a resolution of 4 cm^{-1}. CO_2 adsorption-desorption experiments were performed on an ASAP 2020 Micromeritics Instrument at 25 °C. The samples were activated by evacuation at 100 °C overnight to remove physisorbed gases.

UV-visible spectroscopy. UV-Visible absorption spectra (SHIMADZU UV-3600 Plus UV-VIS-NIR Spectrophotometer) were acquired before and after SIS on PMMA-coated fused quartz substrates. Absorption spectra for PMMA films on fused quartz substrates were subtracted from all experimental sample spectra to correct for substrate reflectivity and the weak absorption of PMMA and fused quartz below 250 nm. Where

relevant, SIS modified substrates were heat treated in a tube furnace under flowing N_2 atmosphere for 30 minutes to promote indium oxyhydroxide dehydration without degradation of the PMMA thin film.

4. RESULTS AND DISCUSSION

Sample Characterization:

TMIn and other group 13 trialkyl metal precursors have been shown to form a reversible adduct with the carbonyl group of PMMA at 80 °C.[16] After a short (5s) purge step to remove gas-phase TMIn, the adducted TMIn in the PMMA host is hypothesized to react with H_2O in a proton-mediated ligand exchange that releases methane. Previous infrared studies reveal that the majority of carbonyl groups are released from adduction upon H_2O exposure and are, therefore, available for TMIn adduct formation in subsequent SIS cycles, Figure 1.[16] However, quenching adducted TMIn in subsequent cycles is likely to seed new clusters, thereby inducing a mixture of cluster sizes. Instead, we adopt a modified growth sequence in which an extended TMIn purge (120s) allows nearly complete adduct dissociation. Consequently, deposition is restricted to the irreversible reaction of TMIn with $InO_x(OH)_y$ clusters nucleated in the first SIS cycles, a process which is purge time independent.

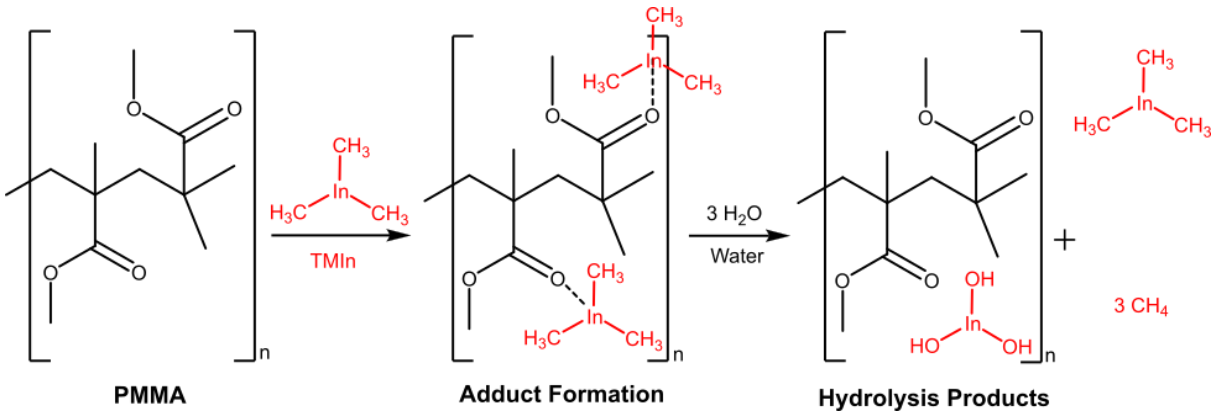

Figure 1. Idealized representation of the first SIS cycle, including adduct formation and reaction with water to produce $In(OH)_3$ and free carbonyl sites in the PMMA matrix.

Previous X-ray characterization and the proposed mechanism for SIS reaction (1) suggest that clusters of $InOx(OH)_y$ formed in the first few SIS cycles may contain structural motifs similar to the crystalline $In(OH)_3$ phase.

$$In(CH_3)_3 + 3H_2O \rightarrow In(OH)_3 + 3CH_4 \qquad (1)$$

We consider the vibrational and optical properties of bulk $In(OH)_3$ and their relationship to the SIS-derived $InOx(OH)_y$ clusters. Previous K-edge EXAFS and PDF analysis of X-ray scattering data of growing $InO_x(OH)_y$ clusters within the PMMA were modelled as multinuclear clusters with coordination environments related to cubic $In(OH)_3$ and cubic In_2O_3.[16] We consider five clusters that are consistent with previous EXAFS and PDF analysis (Scheme 1).

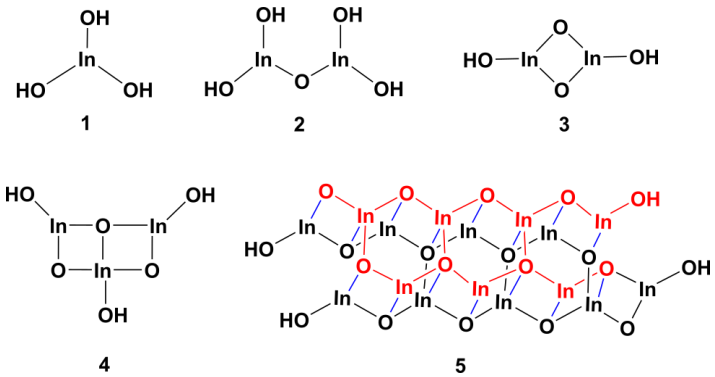

Scheme 1. Proposed $InO_x(OH)_y$ clusters.

The infrared spectrum of a pristine PMMA thin film, Figure 2, reveals the expected features previously assigned to the carbonyl group C=O stretching vibration at 1738 cm^{-1} and the ester group C-O stretching vibrations between 1000 and 1260 cm^{-1}. The peak near 1480 cm^{-1} is assigned to the C=C stretch and the C-H stretching vibrations are visible at 2958 cm^{-1}. Spectra referenced to the pristine PMMA film on Au-coated silicon are provided as Figure S1.

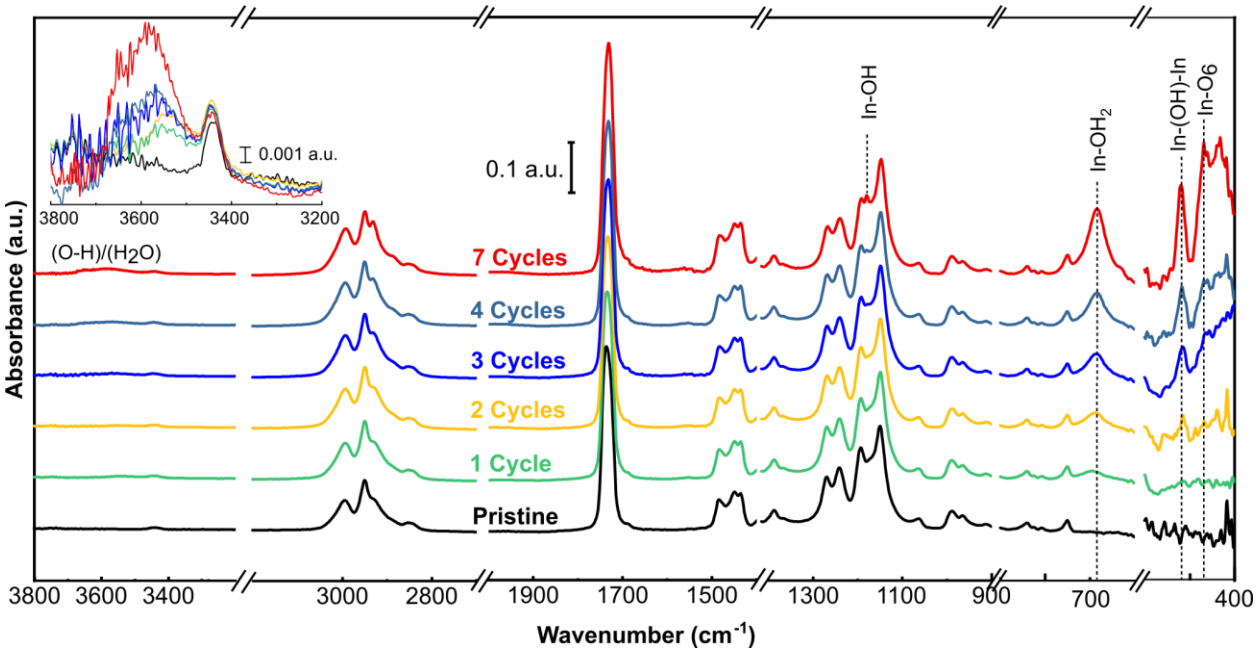

Figure 2. In situ FTIR spectra measured after a variable number of SIS cycles in PMMA films on Ge/Au-coated silicon substrates at 80 °C. Spectra were recorded after a complete 240 second purge after H_2O dosing to ensure complete removal of physisorbed H_2O. All spectra are referenced to Au-coated silicon and are vertically offset for clarity. The peak at 3440 cm^{-1} in the zoomed inset is an overtone band of the carbonyl stretching vibration of PMMA.

The complete purge of physisorbed (or weakly adsorbed) H_2O was confirmed by the absence of a free H_2O bending vibration near 1640 cm^{-1} after each SIS cycle. The regions of interest are associated with $InO_x(OH)_y$ and its chemical interaction with the PMMA matrix. The vibrational analysis is assisted by literature precedent.[16] The spectral region between 400 – 900 cm^{-1}, which is characteristic for metal-oxygen bonding, shows three peaks at 400-500 cm^{-1} (broad), 522 cm^{-1} (sharp), 686 cm^{-1} (broad) that are attributed to the vibrations associated with bulk In_xO_y modes, dimeric (e.g., -In-(OH)-In-), and octahedrally coordinated In-OH_2 species respectively.[17–20] The intensity of these FTIR absorbances increases with increasing SIS cycle number, consistent with an increasing average $InO_x(OH)_y$ cluster size. The lowest wavenumber vibrations associated with bulk In_xO_y modes are not well resolved until after the 2nd SIS cycle, consistent with a majority of isolated $In(OH)_y$ species after the first SIS cycle. The evolution of the structure of the $InO_x(OH)_y$ clusters is inferred from the emergence and absorbance evolution of the IR bands near 684 and 522 cm^{-1} as a function of the number of SIS cycles, Figure 3.

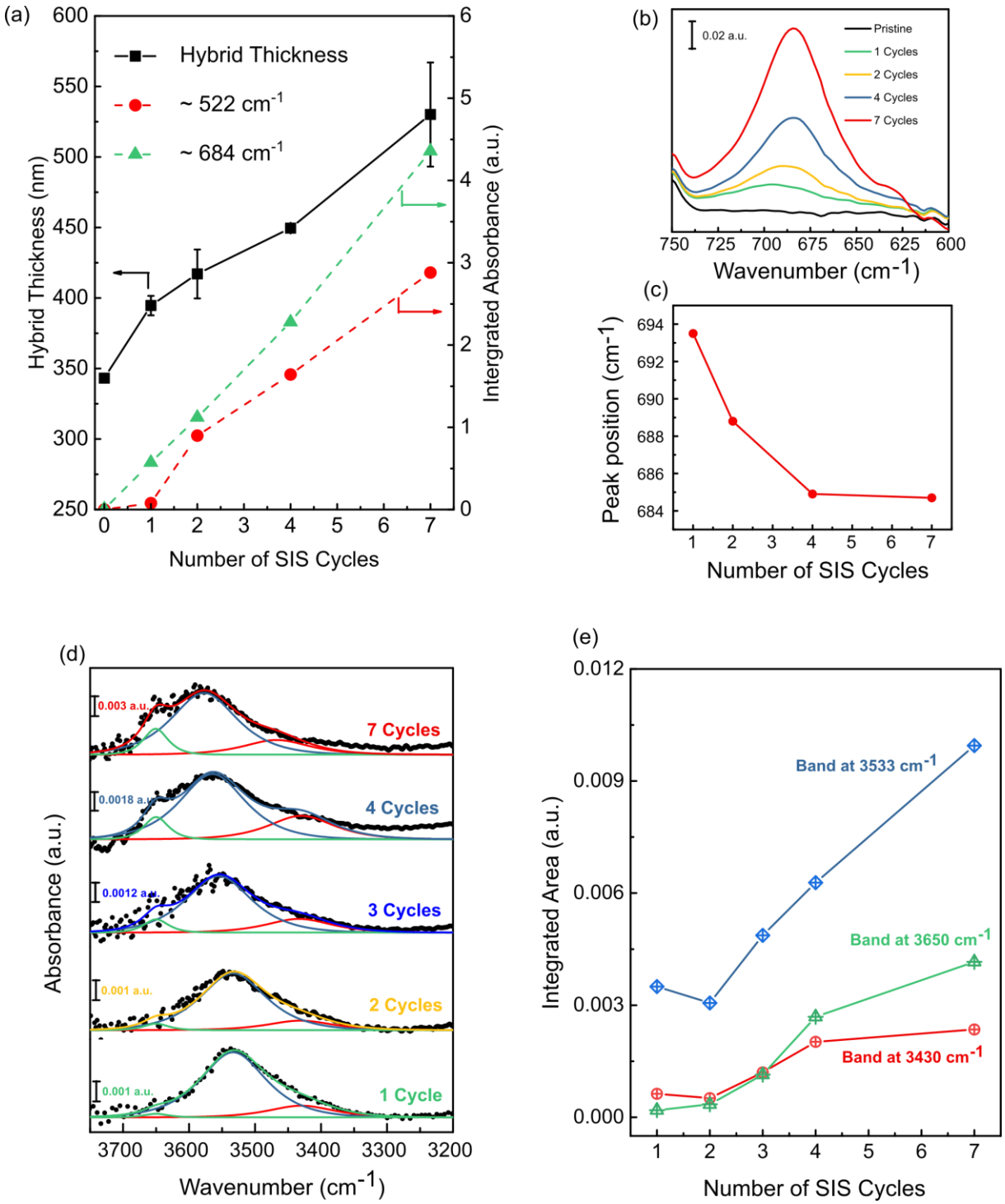

Figure 3. (a) The hybrid film thickness is estimated from spectroscopic ellipsometry as function of SIS cycles numbers. The peak absorbance of In-hydroxyl vibrations also increases with SIS cycle number (b) Expanded view of 750 – 600 cm^{-1} revealing (c) peak position shift. (d) IR absorbance spectra from 3700 – 3200 cm^{-1} in the region of overlapping OH and H_2O stretching vibrations corresponding to different $InO_x(OH)_y$ clusters with spectral deconvolution by curve fitting. (e) Variation of the integrated fitted peak areas as a function of number of SIS cycles for the indicated peak positions.

The integrated absorbance of the modes centered near 684 cm^{-1} increases with the number of SIS cycles, consistent with a greater surface area for each cluster that supports more octahedrally coordinated In-OH_2. Figure 3b shows a red shift in the wavenumber of the In-OH_2 related modes suggesting a weakening of the H_2O adsorption strength as expected for progressively larger clusters. Secondly, the broad In-OH_2 modes may be indicative of an inhomogeneous coordination environment in which some methyl groups are not hydrolyzed and may remain bound to In. The integrated absorbance centered near 522 cm^{-1}, is absent for 1 SIS cycle and is observed for 2 SIS cycles and increases upon further SIS cycles. This band is assigned to dimeric (e.g., -In(-OH)-In-) species that may result from nuclei growth or condensation reactions with neighboring nuclei. The integrated FTIR absorbance for the In_xO_y bulk modes in the 500-400 cm^{-1} region, Figure S2, is also consistent with cluster growth as opposed to additional single-atom nuclei.

The infrared spectra in the region 900 – 1900 cm^{-1} is characterized by the growth of a sharp band near 1180 cm^{-1}. This band may be assigned to the OH deformation vibration characteristic of bulk $In(OH)_3$.[18] The peak at 1180 cm^{-1} is also in the region expected for μ_1-OH hydroxyl species in In-(OH)-In bridging vibrations and is most prominent after 7 SIS cycles. This peak may also be indicative of deformation of the CH_3 and stretching of C–O–C and C–C bonds in PMMA, however this is unlikely since the peak is directly dependent on the SIS process.[18,21] As reported previously, there is minimal perturbation of the carbonyl peak that would be indicative of weak bonding between the carbonyl groups and the $InO_x(OH)_y$ clusters. However, the carbonyl peak is broadened to lower wavenumbers after each SIS cycle, suggesting the possibility of dipole-dipole interactions between $InO_x(OH)_y$ clusters and the carbonyl groups. This effect is more evident in the difference spectra (Figure S1) where a positive peak at ~1728 cm^{-1} without a corresponding bleach that would be expected if carbonyls were bonded to $InO_x(OH)_y$. The region 2800 – 3200 cm^1 is associated with the symmetric and asymmetric stretches of CH_3 and CH_2 bonds on PMMA. The peak perturbations in this region may be indicative of incomplete methyl removal from the In precursor or attributed to microphase changes in PMMA ordering. The high frequency region is characterized by broad, structureless bands near 3580 and 3646 cm^{-1} which are indicative of hydroxyl and/or aqua species. Since the clusters are grown at low temperature (80 °C) and H_2O is used as a precursor the clusters are likely to be extensively hydroxylated. We expect the corresponding FTIR spectra to show multiple -OH stretching vibrations due to the anticipated presence of several types of hydroxyl groups, Scheme 2, in addition to various hydrogen bonding environments within the PMMA matrix and between adjacent clusters. The broad O-H stretching bands also suggest that the growing clusters contain nonstoichiometric coordinated or physisorbed OH/H_2O ligands.

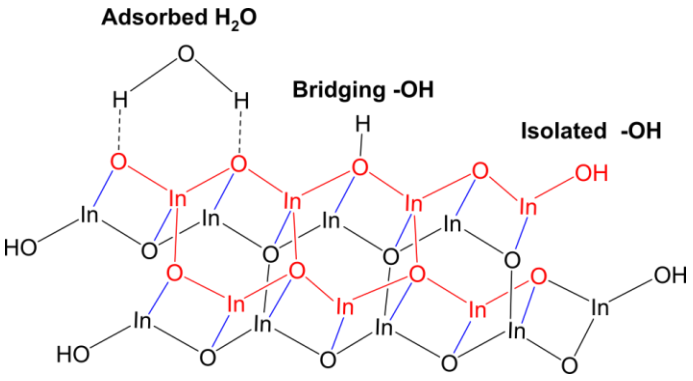

Scheme 2. Proposed reactive sites and hydroxyl groups present on large $InO_x(OH)_y$ structures

To probe the evolution of the hydroxyl stretching vibrations as a function of the number of SIS cycles, the FTIR difference spectra was calculated after each SIS cycle with reference to pristine PMMA (Figure 3d). The calculated difference spectra were further deconvoluted into multiple peaks using mixed Gaussian-Lorentzian functions with factor 0.75 and fixed FWHM while all other parameters were free. All spectra were fit to three such peaks where the two broad and structureless bands centered near 3650 cm^{-1} and 3533 cm^{-1} are assign broadly to the O-H stretching vibrations of In-OH and coordinated H_2O respectively.[18,20] The intensity of the two O-H streching peaks increases with SIS cycle number, consistent with the expected increase in cluster size and surface area . The broadness indicated by full width at half-maximum (FWHM) values greater than 50 cm^{-1} suggest that the hydroxyl groups on these $InO_x(OH)_y$ clusters are non-uniform and experience multiple hydrogen bonding environments. The

growth of a high energy shoulder around 3650 cm^{-1} points to isolated or weakly H-bonded hydroxyl groups growing on well-defined polycationic structures similar to that in Scheme 1[15] or reported in cage-like Al_{13} Keggin clusters.[22] Finally, as the $InO_x(OH)_y$ are very small in small in size, they are likely to have a disproportionately large fraction of water adsorbed to the relatively large surface area as seen in the low frequency peak band centered at 3430 cm^{-1} in the range associated with weakly coordinated H_2O and/or hydroxyl groups experienced extensive H-bonding. It is noteworthy that the deconvolution and integration of the O-H stretching vibration bands may inaccurately estimate the nature and/or population of hydroxyl groups due to extensive hydrogen bonding likely across the variable cluster sizes. Nonetheless, the band areas at 3533 and 3650 cm^{-1} show a similar increase with each additional SIS cycle.

Optical Properties of PMMA-$InO_x(OH)_y$ Hybrids

The optical properties of $InO_x(OH)_y$ clusters in PMMA matrix were investigated by ex situ measurement of the UV-vis absorbance spectra of SIS-derived hybrid films at room temperature. The hybrid films are transparent to visible wavelengths but strongly absorb below 300 nm with absorptivity that increases with additional SIS cycles, Figure 4, as expected for the increasing inorganic component embedded within the PMMA matrix. In contrast to typical thin film growth, the onset energy and characteristic spectral shape of the clusters show a strong dependence on SIS cycles number, and by extension, $InO_x(OH)_y$ cluster size. The high energy absorption onset ranging from 250 – 300 nm suggests the existence of finite size clusters (few-metal atom species rather than bulk *bcc*-indium oxide, which exhibits a direct band gap in the range of 3.6 – 3.7 eV (335 – 345 nm).[23,24] Such behavior has also been observed in the nanomeric oxides of vanadium[25] and copper[26]. Indium hydroxides and oxyhydroxides are n-type semiconductors with band gaps reported to cover a much wider range, 3.0 – 5.5 eV, corresponding to 226 to 414 nm.[6,27,28] Body-centered cubic $In(OH)_3$ was previously shown to exhibit two absorption peaks centered at 222 (large) and 300 nm (smaller).[28,29]

The band gap energy of SIS-derived clusters was estimated using the Tauc relation

$$\alpha h\nu = B\left(h\nu - E_g\right)^n \qquad (2)$$

where α is the absorption coefficient, $h\nu$ is the photon energy, E_g is the optical band gap energy, B is a proportionality constant, and n is a constant with value of ½ for indirect bandgap transitions. The absorption coefficient, α, is defined as

$$\alpha = 2.303\frac{A}{t} \qquad (3)$$

where A is the absorbance and t is the effective thickness of $InO_x(OH)_y$ clusters estimated from the composition fraction of $InO_x(OH)_y$ in PMMA multiplied by the total thickness after SIS as deduced from spectroscopic ellipsometry.

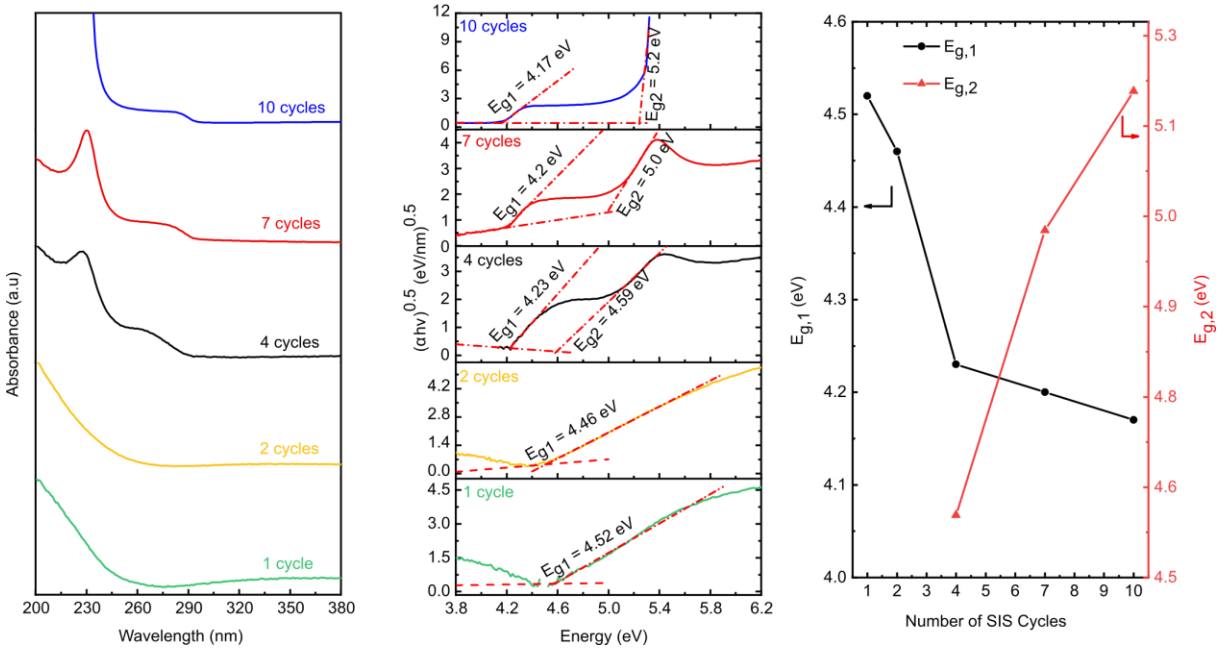

Figure 4. (a) The UV-vis absorption spectra of $InO_x(OH)_y$ for various SIS cycles stabilized in PMMA matrix and dried at 80 °C. The vertically offset spectra are corrected for the absorbance of PMMA and fused quartz substrate. (b) Tauc plot for direct transition (n = ½) for $InO_x(OH)_y$ clusters stabilized in PMMA matrix. (c) Direct transition optical band gap energies as a function of SIS cycle number.

Figure 4 shows that the smallest clusters, derived from 1 or 2 SIS cycles, exhibit featureless absorption spectra with onset at approximately 250 nm (5.0 eV). Such featureless absorption is indicative of non-crystalline $InO_x(OH)_y$ species lacking extended structure. However, with additional SIS cycles including 4, 7 and 10, two sharper absorption peaks at ~230 nm (5.4 eV) and ~280 nm (4.4 eV) emerge to eventually dominate the spectral shape. Sharp absorption features that occur at consistent wavelengths are consistent with the lowest energy electronic transition of "finite size clusters".[30] Since the intensity of the band at 230 nm appears to increase with the number of SIS cycles i.e. $InO_x(OH)_y$ effective thickness in each sample, this peak is broadly assigned to $InO_x(OH)_y$ species. While the direct and indirect band gap energies of PMMA thin films have been reported to be near 5.0 eV and 4.8 eV respectively,[31] neither the PMMA effective film thickness nor its absorptivity are expected to change with the incorporation of $InO_x(OH)_y$ such that the subtracted spectra shown are assigned to $InO_x(OH)_y$ absorption alone.

The appearance of sharp absorption features at 4 SIS cycles suggests a change in the coordination environment of the indium as the cluster size increases. The features of the UV-vis spectra can be understood if the OH present on the $InO_x(OH)_y$ are treated as ligands capable of ligand-to-metal charge-transfer (MLCT) character. The sharp band centered near 230 nm, reminiscent of molecular-like absorbance features, is assigned to an LMCT transition from oxygen in hydroxyl ligands to isolated or monomeric $[In]^{3+}$ centers. Considering the low absorbance of this band after the first two SIS cycles, the $[In]^{3+}$ ions would have to be extensively dispersed in the PMMA matrix without any significant order, as suggested previously.[15,32] The band near 280 nm redshifts with increasing SIS cycles as well as increases in intensity. We hypothesize this band to originate from LMCT from oxygen to $[In]^{3+}$ albeit in μ_2-OH moiety as is present in the larger, oligomeric $InO_x(OH)_y$ clusters. Based on the optical properties of indium exchanged zeolite[32,33] and indium doped alkali halide solids[34,35], this absorption band is also indicative of $[In]^{3+}$ cations in an octahedral coordination sphere of O atoms, i.e. $[InO_6]$ as proposed in the structure of the largest $InO_x(OH)_y$ clusters (7 and 10 SIS cycles). There is an inverse relationship between the number of SIS cycles and the lowest energy band gap energy ($E_{g,1}$), Figure 4c. In contrast, the highest energy band gap ($E_{g,2}$) increases with SIS cycle number. The redshift in the lowest energy (i.e. band edge) is ascribed to an increasing size and aspect ratio of the $InO_x(OH)_y$ clusters. Furthermore, it appears that the intensity of the band centered near 280 nm slightly decreases after 4 SIS cycles.

Cluster Evolution - Thermal Dehydroxylation under N_2 Atmosphere

Previous studies of TMIn/H_2O SIS films fired to > 250 °C in air reveal the burnout of PMMA as well as densification + crystallization of the inorganic component to In_2O_3.[36] However, at lower temperatures and in the absence of oxygen the PMMA component is expected to remain largely intact while the cluster structure and surface chemistry may evolve.[37] We investigate the influence of low temperature treatment at temperatures up to 250 °C in a N_2 atmosphere. Thermal treatment up to 200 °C does not exhibit significant changes in the UV/vis spectra, except for minor decreases in the optical bandgap energies (less than 0.05 eV), Figure 5. This suggests that the embedded clusters exhibit stability up to at least 200 °C in inert atmospheres. However, treatment at 250 °C induces pronounced changes in the optical properties. First, the intensity of the absorption band near 230 nm ($E_{g,2}$) progressively decreases with increasing annealing temperature, consistent with condensation and agglomeration of neighboring $In(OH)_y$ species forming oligomeric (M-O-M networks) nanostructures and ultimately bulk and amorphous $In(OH)_3$ or In_2O_3 "like" nanocrystals.[16,36,38,39] The optical band gap energy (3.63 eV) for the PMMA-$InO_x(OH)_y$ hybrids treated at 250 °C is similar to bulk In_2O_3 (3.75 eV)[40] but not crystalline $In(OH)_3$ (5.15 eV).[28] The formation of crystalline In_2O_3 would also be consistent with previous reports of crystalline In_2O_3 formed upon $InO_x(OH)_y$-PMMA films annealed in air at a similar temperature of 300 °C.

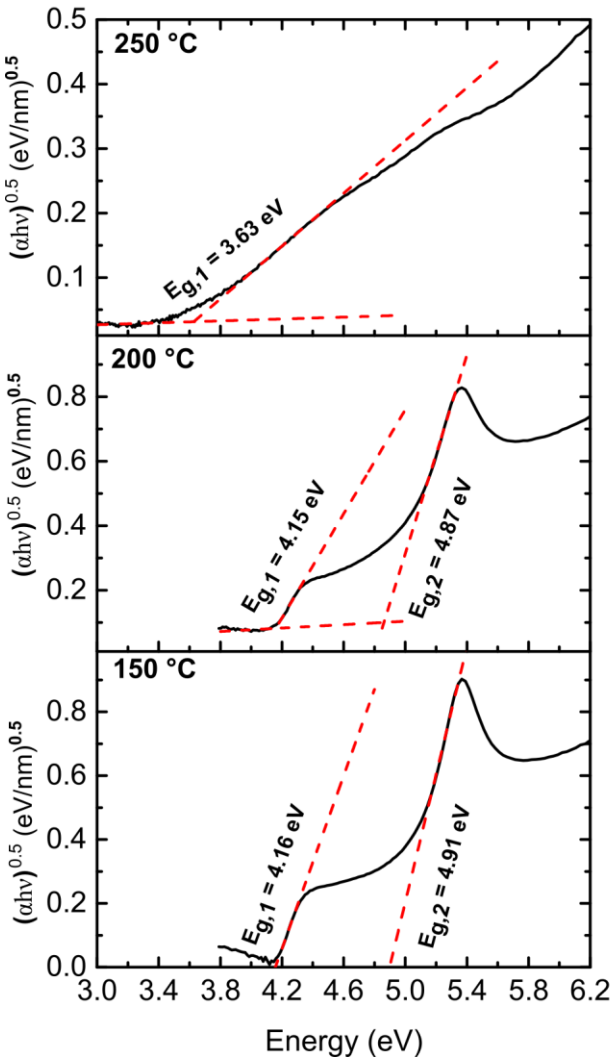

Figure 5. Tauc plots for 7 SIS cycle samples after annealing for 30 minutes under flowing N_2 atmosphere at different temperatures.

CO_2 Adsorption Studies

As indium hydroxide is a well-known catalyst for CO_2 electroreduction,[7] we propose that $InO_x(OH)_y$ clusters stabilized in PMMA matrix might also serve as platform for CO_2 binding. The proposed structure of the $InO_x(OH)_y$ clusters exhibit a rich population of Lewis acid and base sites (OH^- and In^{3+} respectively). Related molecular motifs have been shown to be catalytically active for CO_2 conversion.[41–45] Owing to the hydroxyl-rich nature of the clusters formed after 7 SIS cycles in PMMA, we preliminarily probed the CO_2 adsorption of this material for CO_2 capture potential applications. Briefly, silicon oxide wafers (0.5 cm^2) with pristine and SIS modified PMMA were activated at 100 °C under vacuum for 12 hours. CO_2 adsorption isotherms (volume of gas adsorbed per mass of Si wafer + PMMA + $InO_x(OH)_y$ as a function of pressure) were measured at room temperature (295.15 K) (Figure 7). The SIS modified PMMA exhibits approximately 28% enhancement in CO_2 adsorption compared to pristine PMMA at 1 bar. The enhanced CO_2 adsorption may be a consequence of more attractive interactions between CO_2 and the hydroxyl groups of the $InO_x(OH)_y$ clusters relative to the acrylate groups in pristine PMMA.[46,47] The details of CO_2 adsorption on SIS-modified PMMA are the subject of future investigations.

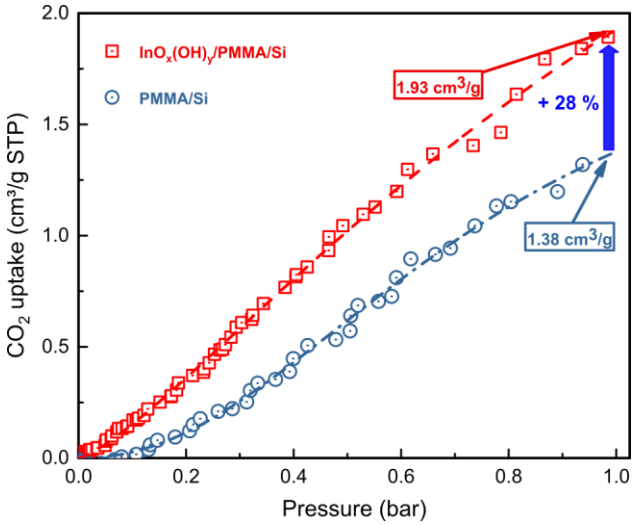

Figure 7: CO_2 adsorption isotherms on pristine and $InO_x(OH)_y$ modified PMMA films on a silicon wafer support. Note: Sample mass includes the weight of the Si wafer support.

CONCLUSIONS

$InO_x(OH)_y$ synthesized within a PMMA matrix exhibit SIS-cycle-number-dependent chemical and physical properties. In the few cycle limit, the results are consistent with size-dependent few atom clusters that exhibit unique optical properties intermediate between $In(OH)_3$ and cubic In_2O_3. Preliminary CO_2 adsorption isotherms reveal that the $InO_x(OH)_y$ clusters moderately enhance CO_2 uptake compared to pristine PMMA. This observation can be attributed to Lewis acid-base interactions between CO_2 and In-OH or In-OH_2 species moieties. We hypothesize that polymer modification with metal oxyhydroxide clusters via sequential infiltration synthesis (SIS) may provide a strategy to improve the gas adsorption performance of simple polymers including as PMMA.

ACKNOWLEDGEMENTS

This work is supported by the U.S. Department of Energy (DOE), Office of Science, Office of Basic Energy Science, Division of Chemical Sciences, Geosciences, and Biosciences, through Argonne National Laboratory under Contract No. FWP 34698

REFERENCES

(1) Waldman, R. Z.; Mandia, D. J.; Yanguas-Gil, A.; Martinson, A. B. F.; Elam, J. W.; Darling, S. B. The Chemical Physics of Sequential Infiltration Synthesis—A Thermodynamic and Kinetic Perspective. *J. Chem. Phys.* **2019**, *151* (19), 190901. https://doi.org/10.1063/1.5128108.

(2) Cara, E.; Murataj, I.; Milano, G.; De Leo, N.; Boarino, L.; Ferrarese Lupi, F. Recent Advances in Sequential Infiltration Synthesis (SIS) of Block Copolymers (BCPs). *Nanomaterials* **2021**, *11* (4), 994.

https://doi.org/10.3390/nano11040994.
(3) Leng, C. Z.; Losego, M. D. Vapor Phase Infiltration (VPI) for Transforming Polymers into Organic-Inorganic Hybrid Materials: A Critical Review of Current Progress and Future Challenges. *Mater. Horizons* **2017**, *4* (5), 747–771. https://doi.org/10.1039/c7mh00196g.
(4) Peng, Q.; Tseng, Y. C.; Darling, S. B.; Elam, J. W. A Route to Nanoscopic Materials via Sequential Infiltration Synthesis on Block Copolymer Templates. *ACS Nano* **2011**, *5* (6), 4600–4606. https://doi.org/10.1021/nn2003234.
(5) Wilson, C. A.; Grubbs, R. K.; George, S. M. Nucleation and Growth during Al_2O_3 Atomic Layer Deposition on Polymers. *Chem. Mater.* **2005**, *17* (23), 5625–5634. https://doi.org/10.1021/cm050704d.
(6) Zhuang, Z.; Peng, Q.; Liu, J.; Wang, X.; Li, Y. Indium Hydroxides, Oxyhydroxides, and Oxides Nanocrystals Series. *Inorg. Chem.* **2007**, *46* (13), 5179–5187. https://doi.org/10.1021/ic061999f.
(7) Li, J.; Zhu, M.; Han, Y. Recent Advances in Electrochemical CO_2 Reduction on Indium-Based Catalysts. *ChemCatChem* **2021**, *13* (2), 514–531. https://doi.org/10.1002/cctc.202001350.
(8) Tsai, C. J.; Jordan, K. D.; Schutz, M.; Burgi, T.; Leutwyler, S.; BOrgi, H. B.; Baker, T.; Dodson, E.; Dodson, G.; Hodgkin, D.; Hubbard, R.; Crystallography in Molecular Biology, in; Moras, D.; Drenth, J.; Strandberg, B.; Suc, D.; Wilson, K.; Page, H.; Frey, J. G.; Shen, Y.; Lee, Y. T.; Buckingham, D.; Wales, D.; Alivisatos, A. P. Semiconductor Clusters, Nanocrystals, and Quantum Dots. *Science (80-.).* **1996**, *271* (5251), 933–937. https://doi.org/10.1126/SCIENCE.271.5251.933.
(9) Nielsen, I. G.; Sommer, S.; Iversen, B. B. Phase Control for Indium Oxide Nanoparticles. *Nanoscale* **2021**, *13* (7), 4038–4050. https://doi.org/10.1039/d0nr08587a.
(10) Asmis, K. R.; Fielicke, A. Size-Selected Clusters as Model Systems for Catalysis. *Top. Catal.* **2018**, *61*, 1–2. https://doi.org/10.1007/s11244-018-0906-5.
(11) Lu, P.; Tan, X.; Zhao, H.; Xiang, Q.; Liu, K.; Zhao, X.; Yin, X.; Li, X.; Hai, X.; Xi, S.; Wee, A. T. S.; Pennycook, S. J.; Yu, X.; Yuan, M.; Wu, J.; Zhang, G.; Smith, S. C.; Yin, Z. Atomically Dispersed Indium Sites for Selective CO_2 Electroreduction to Formic Acid. *ACS Nano* **2021**, *15* (3), 5671–5678. https://doi.org/10.1021/acsnano.1c00858.
(12) Sheldon, R. A.; Arenas, I. W. C. E. Organocatalytic Oxidations Mediated by Nitroxyl Radicals. *Adv. Synth. Catal.* **2004**, *346* (9–10), 1051–1071. https://doi.org/10.1002/adsc.200404110.
(13) Pu, Z.; Amiinu, I. S.; Cheng, R.; Wang, P.; Zhang, C.; Mu, S.; Zhao, W.; Su, F.; Zhang, G.; Liao, S.; Sun, S. Single-Atom Catalysts for Electrochemical Hydrogen Evolution Reaction: Recent Advances and Future Perspectives. *Nano-Micro Letters*. **2020**. https://doi.org/10.1007/s40820-019-0349-y.
(14) Wang, A.; Li, J.; Zhang, T. Heterogeneous Single-Atom Catalysis. *Nat. Rev. Chem.* **2018**, *2* (6), 65–81. https://doi.org/10.1038/s41570-018-0010-1.
(15) He, X.; Waldman, R. Z.; Mandia, D. J.; Jeon, N.; Zaluzec, N. J.; Borkiewicz, O. J.; Ruett, U.; Darling, S. B.; Martinson, A. B. F.; Tiede, D. M. Resolving the Atomic Structure of Sequential Infiltration Synthesis Derived Inorganic Clusters. *ACS Nano* **2020**, *14* (11), 14846–14860. https://doi.org/10.1021/acsnano.0c03848.
(16) Waldman, R. Z.; Jeon, N.; Mandia, D. J.; Heinonen, O.; Darling, S. B.; Martinson, A. B. F. F. Sequential Infiltration Synthesis of Electronic Materials: Group 13 Oxides via Metal Alkyl Precursors. *Chem. Mater.* **2019**, *31* (14), 5274–5285. https://doi.org/10.1021/acs.chemmater.9b01714.
(17) Yang, J.; Frost, R. L.; Martens, W. N. Thermogravimetric Analysis and Hot-Stage Raman Spectroscopy of Cubic Indium Hydroxide. *J. Therm. Anal. Calorim.* **2010**, *100* (1), 109–116. https://doi.org/10.1007/s10973-009-0554-x.
(18) Yang, J. (Jeanne); Cheng, H.; Martens, W. N.; Frost, R. L. Application of Infrared Emission Spectroscopy to the Thermal Transition of Indium Hydroxide to Indium Oxide Nanocubes. *Appl. Spectrosc.* **2011**, *65* (1), 113–118. https://doi.org/10.1366/10-06082.
(19) Robinson, J. W. *Practical Handbook of Spectroscopy*; CRC Press: Florida, **2000**.
(20) Wang, X.; Andrews, L. Infrared Spectroscopic Observation of the Group 13 Metal Hydroxides, $M(OH)_{1,2,3}$ (M =Al, Ga, In, and Tl) and $HAl(OH)_2$. *J. Phys. Chem. A* **2007**, *111* (10), 1860–1868. https://doi.org/10.1021/jp066390e.
(21) Kharlanov, A. N.; Turakulova, O. A.; Lunin, V. V. Effect of Indium Oxide Modification on the Phase Composition, the Structure of a Hydroxyl Cover, and the Electron-Acceptor Properties of Zirconium Dioxide. *Kinet. Catal.* **2004**, *45* (2), 260–265. https://doi.org/10.1023/B:KICA.0000023801.86194.d8.
(22) Casey, W. H. Large Aqueous Aluminum Hydroxide Molecules. *Chem. Rev*. **2006**, *106*, 1–16.

https://doi.org/10.1021/cr040095d.
(23) Köstlin, H.; Jost, R.; Lems, W. Optical and Electrical Properties of Doped In_2O_3 Films. *Phys. Status Solidi* **1975**, *29* (1), 87–93. https://doi.org/10.1002/pssa.2210290110.
(24) Weiher, R. L.; Ley, R. P. Optical Properties of Indium Oxide. *J. Appl. Phys.* **1966**, *37* (1), 299–302. https://doi.org/10.1063/1.1707830.
(25) Bulánek, R.; Čapek, L.; Setnička, M.; Čičmanec, P. DR UV-Vis Study of the Supported Vanadium Oxide Catalysts. *J. Phys. Chem. C* **2011**, *115* (25), 12430–12438. https://doi.org/10.1021/jp112206c.
(26) Bravo-Suárez, J. J.; Subramaniam, B.; Chaudhari, R. V. Ultraviolet-Visible Spectroscopy and Temperature-Programmed Techniques as Tools for Structural Characterization of Cu in $CuMgAlO_x$ Mixed Metal Oxides. *J. Phys. Chem. C* **2012**, *116* (34), 18207–18221. https://doi.org/10.1021/jp303631v.
(27) Ito, N.; Sato, Y.; Song, P. K.; Kaijio, A.; Inoue, K.; Shigesato, Y. Electrical and Optical Properties of Amorphous Indium Zinc Oxide Films. *Thin Solid Films* **2006**, *496* (1), 99–103. https://doi.org/10.1016/j.tsf.2005.08.257.
(28) Avivi, S.; Mastai, Y.; Gedanken, A. Sonohydrolysis of In^{3+} Ions: Formation of Needlelike Particles of Indium Hydroxide. *Chem. Mater.* **2000**, *12* (5), 1229–1233. https://doi.org/10.1021/cm9903677.
(29) Yan, T.; Li, W.; Bi, S.; You, J. Effects of Annealing on the Microstructures and UV and Visible Light-Induced Photocatalytic Activities of Indium Hydroxide Nanocubes. *J. Nanosci. Nanotechnol.* **2015**, *15* (3), 2197–2203. https://doi.org/10.1166/jnn.2015.9224.
(30) Kim, B. H.; Hackett, M. J.; Park, J.; Hyeon, T. Synthesis, Characterization, and Application of Ultrasmall Nanoparticles. *Chem. Mater.* **2014**, *26* (1), 59–71. https://doi.org/10.1021/cm402225z.
(31) Aziz, S. B.; Abdullah, O. G.; Hussein, A. M.; Ahmed, H. M. From Insulating PMMA Polymer to Conjugated Double Bond Behavior: Green Chemistry as a Novel Approach to Fabricate Small Band Gap Polymers. *Polymers (Basel).* **2017**, *9* (11), 626. https://doi.org/10.3390/polym9110626.
(32) Serykh, A. I. Optical Properties of Indium-Exchanged Mordenite Zeolite. *Microporous Mesoporous Mater.* **2019**, *275*, 147–151. https://doi.org/10.1016/j.micromeso.2018.08.024.
(33) Serykh, A. I.; Rozhdestvenskaya, N. N. Photoluminescence Properties of Indium-Exchanged ZSM-5 Zeolite. *J. Phys. Chem. C* **2015**, *119* (31), 17612–17618. https://doi.org/10.1021/acs.jpcc.5b01387.
(34) Ranfagni, A.; Mugnai, D.; Bacci, M.; Viliani, G.; Fontana, M. P. The Optical Properties of Thallium-like Impurities in Alkali-Halide Crystals. *Adv. Phys.* **1983**, *32* (6), 823–905. https://doi.org/10.1080/00018738300101621.
(35) Jacobs, P. W. M. Alkali Halide Crystals Containing Impurity Ions with the ns^2 Ground-State Electronic Configuration. *J. Phys. Chem. Solids* **1991**, *52* (1), 35–67. https://doi.org/10.1016/0022-3697(91)90059-9.
(36) Taggart, A. D.; Jeon, N.; Rozyyev, V.; Karapetrova, E.; Zaluzec, N. J.; Waldman, R. Z.; Darling, S. B.; Elam, J. W.; Martinson, A. B. F. Electronic Conductivity of Nanoporous Indium Oxide Derived from Sequential Infiltration Synthesis. *J. Phys. Chem. C* **2021**, *125* (38), 21191–21198. https://doi.org/10.1021/acs.jpcc.1c06103.
(37) Peterson, J. D.; Vyazovkin, S.; Wight, C. A. Kinetic Study of Stabilizing Effect of Oxygen on Thermal Degradation of Poly(Methyl Methacrylate). *J. Phys. Chem. B* **1999**, *103* (38), 8087–8092. https://doi.org/10.1021/jp991582d.
(38) Yan, T.; Long, J.; Shi, X.; Wang, D.; Li, Z.; Wang, X. Efficient Photocatalytic Degradation of Volatile Organic Compounds by Porous Indium Hydroxide Nanocrystals. *Environ. Sci. Technol.* **2010**, *44* (4), 1380–1385. https://doi.org/10.1021/es902702v.
(39) Chu, D.; Zeng, Y.-P.; Jiang, D.; Xu, J. Tuning the Phase and Morphology of In_2O_3 Nanocrystals via Simple Solution Routes. **2007**. https://doi.org/10.1088/0957-4484/18/43/435605.
(40) Yu, D.; Yu, S. H.; Zhang, S.; Zuo, J.; Wang, D.; Qian, Y. Metastable Hexagonal In_2O_3 Nanofibers Templated from InOOH Nanofibers under Ambient Pressure. *Adv. Funct. Mater.* **2003**, *13* (6), 497–501. https://doi.org/10.1002/adfm.200304303.
(41) Ghuman, K. K.; Hoch, L. B.; Szymanski, P.; Loh, J. Y. Y.; Kherani, N. P.; El-Sayed, M. A.; Ozin, G. A.; Singh, C. V. Photoexcited Surface Frustrated Lewis Pairs for Heterogeneous Photocatalytic CO_2 Reduction. *J. Am. Chem. Soc.* **2016**, *138* (4), 1206–1214. https://doi.org/10.1021/jacs.5b10179.
(42) Ghuman, K. K.; Wood, T. E.; Hoch, L. B.; Mims, C. A.; Ozin, G. A.; Singh, C. V. Illuminating CO_2 Reduction on Frustrated Lewis Pair Surfaces: Investigating the Role of Surface Hydroxides and Oxygen Vacancies on Nanocrystalline $In_2O_{3-x}(OH)_Y$. *Phys. Chem. Chem. Phys.* **2015**, *17* (22), 14623–14635.

https://doi.org/10.1039/c5cp02613j.
(43) Ghuman, K. K.; Hoch, L. B.; Wood, T. E.; Mims, C.; Singh, C. V.; Ozin, G. A. Surface Analogues of Molecular Frustrated Lewis Pairs in Heterogeneous CO_2 Hydrogenation Catalysis. *ACS Catal.* **2016**, *6* (9), 5764–5770. https://doi.org/10.1021/acscatal.6b01015.
(44) Li, T.; Zhang, W.; Qin, H.; Lu, L.; Yan, S.; Zou, Z. Inorganic Frustrated Lewis Pairs in Photocatalytic CO_2 Reduction. *ChemPhotoChem* **2021**, *5* (6), 495–501. https://doi.org/10.1002/cptc.202000312.
(45) Wang, X.; Lu, L.; Wang, B.; Xu, Z.; Xin, Z.; Yan, S.; Geng, Z.; Zou, Z. Frustrated Lewis Pairs Accelerating CO_2 Reduction on Oxyhydroxide Photocatalysts with Surface Lattice Hydroxyls as a Solid-State Proton Donor. *Adv. Funct. Mater.* **2018**, *28* (43), 1804191. https://doi.org/10.1002/adfm.201804191.
(46) Kazarian, S. G.; Vincent, M. F.; Bright, F. V; Liotta, C. L.; Eckert, C. A. Specific Intermolecular Interaction of Carbon Dioxide with Polymers. *J. Am. Chem. Soc.* **1996**, *118* (7), 1729–1736. https://doi.org/10.1021/ja950416q.
(47) Eslami, H.; Kesik, M.; Karimi-Varzaneh, H. A.; Müller-Plathe, F. Sorption and Diffusion of Carbon Dioxide and Nitrogen in Poly(Methyl Methacrylate). *J. Chem. Phys.* **2013**, *139* (12). https://doi.org/10.1063/1.4821585.